Available online at www.sciencedirect.com

ScienceDirect

JOURNAL OF IRON AND STEEL RESEARCH, INTERNATIONAL. 2016, 23(3): 253-260

Microstructure and Mechanical Properties of NANOBAIN Steel

Yao HUANG[1], Xue-li ZHANG[2], Wei-ning LIU[3], Xu-min WANG[1], Jun-ke HAN[1]

(1. China Electric Power Research Institute, Beijing 100192, China; 2. Beijing Electric Power Design Institute, Beijing 100055, China; 3. AC Construction Branch, State Grid Corporation of China, Beijing 100031, China)

Abstract: The microstructure and mechanical properties of NANOBAIN steel treated at different isothermal temperatures were investigated by scanning electron microscopy (SEM), transmission electron microscopy (TEM), uniaxial tensile tests and X-ray diffraction (XRD). It was found that bainitic ferrite (BF) plate was made of basic shear transformation units arranged in the same direction of subunits. The existence of defects, such as nanoscale twinning and dislocation, suggested that the growth of transformation units was controlled by the surrounding defect plane with dislocation, which was consistent with the moving direction of BF/austenite interface parallel to the twinning plane. The behavior of work hardening indicated that mechanical stability of microstructures obtained at 250 ℃ and 300 ℃ was much more stable than that obtained at 210 ℃. The evolution of carbon partitioning in retained austenite and bainitic ferrite also indicated that austenite was enriched in carbon at the initial stage step by step; after the formation of BF, the austenite did not seem to be greatly enriched in carbon and the carbon content showed a little decrease instead; subsequently, a phenomenon of little decarburization of supersaturated bainitic ferrite has also been found.

Key words: NANOBAIN steel; shear transformation unit; work hardening behavior; carbon partitioning

Since the development of high-strength steels generally involves a compromise between strength and toughness, the refinement of microstructure[1] is the exclusive method to achieve both strength and toughness at present, as all other strengthening mechanisms such as precipitation hardening harm the toughness[2,3]. A brand-new generation of steels now under development, known as NANOBAIN steel, appears to offer notable strength (2.3 GPa), good toughness (30 MPa · $m^{1/2}$) and ductility (up to 25%) in both quasistatic and dynamic loading conditions[4,5]. It is of great potentiality in wide range of utilization in the field of transport, construction and defense. The excellent combination of mechanical properties seems to be partly due to the formation of nanoscale microstructure consisting of very fine bainitic ferrite (BF) plates with an average thickness of 50 nm and film type retained austenite between these BF plates[6].

The mechanical properties of NANOBAIN steel are mainly determined by the morphology of BF and retained austenite. To discuss the morphology of retained austenite, it is of high priority to distinguish the blocky retained austenite and film type retained austenite. The former is bounded by crystallographic variants of bainites heaves with triangular shape in two-dimensional sections while the latter is located between the subunits within a given sheaf of BF. It is well known that a further improvement of ductility can be achieved by a transformation-induced plasticity (TRIP) effect[7,8]; hence, it is necessary to study the work hardening behavior of NANOBIAN steel. Moreover, since nanoscale microstructure and work hardening behavior are closely related with the shape deformation and carbon partitioning[9,10], tensile test curves were studied in detail and carbon contents in retained austenite and BF were examined by X-ray diffraction (XRD) to study the evolution of carbon partitioning.

1 Experimental Procedure

The designed steel was cast as a cylinder bar with diameter of 50 mm and length of 600 mm by utilizing a high frequency induction furnace under argon gas atmosphere. The cast cylinder was electro-slag remelted (ESR) to obtain clean steel. The chemical compositions of steel are shown in Table 1. The steel

Foundation Item: Item Sponsored by National Natural Science Foundation of China (51271035)

Biography: Yao HUANG, Doctor, Engineer; **E-mail**: taohua-daozhu@163.com; **Received Date**: June 24, 2015

Table 1 Chemical compositions in NANOBAIN steel

	C	Si	Mn	Mo	Cr	Co	Al
Mass percent/%	0.75	1.77	2.10	0.27	1.47	1.47	1.21
Atomic percent/%	3.30	3.33	2.02	0.15	1.49	1.32	2.37

after casting and homogenization heat treatment at 1 250 ℃ for 8 h was hot rolled to 4 mm thick plate followed by air cooling. Specimens selected from hot rolled plates were austenitized at 1 000 ℃ for 30 min and then isothermally transformed at different temperatures for different time before quenching into water.

Samples for optical metallography were selected from hot rolled plates and then mechanically polished and etched in a 4% nital solution. The microstructures were characterized using a Zeiss Ultra 55 scanning electron microscope (SEM). Transmission electron microscope (TEM) samples were prepared from 0.30 mm thick discs sliced from tensile testing specimens and observed by a JEOL JEM-2010 transmission electron microscope equipped with a CCD camera operated at 200 kV. The discs were thinned to 0.05 mm by abrasion on SiC papers and then twin jet electro-polished using a solution containing 5 vol.% perchloric acid, 5 vol.% glycerol, and 90 vol.% ethanol at the temperature of −17.5 ℃ and the voltage of 45 V.

Tensile experiments were carried out at room temperature according to GB/T 228—87 with specimens prepared by a milling process. Tensile speed was 0.1 mm/s, corresponding to approximately 0.004 s^{-1} in the engineering strain rate. All samples were machined from the softened bulk material after homogenization and subsequently heat-treated to desired conditions. Engineering stress-engineering strain curves and elongations measured during uniaxial tensile tests were converted to true stress-true strain curves. From the engineering stress-engineering strain curves, offset yield strength (YS) and ultimate tensile strength (UTS) were obtained. Strain hardening was characterized by the incremental strain hardening exponent defined as: $n=\mathrm{d}(\ln\sigma)/\mathrm{d}(\ln\varepsilon_p)$, where n represents work hardening value, ε_p represents true strain, σ represents true stress and $\sigma = k\varepsilon_p^n$, and k is the strength coefficient.

The volume of retained austenite and its carbon content were estimated by quantitative XRD analysis. Samples were machined to be 15 mm×15 mm in dimensions, ground and polished, and then subjected to several cycles of etching and polishing in colloidal silica to obtain an undeformed surface. The prepared samples were then step-scanned in a Rigaku DMAX-RB 12 kW X-ray diffractometer using unfiltered CuKα radiation with a current of 150 mA and a voltage of 40 keV. XRD data was collected over a 2θ range of 10°—100°. The fraction of retained austenite and BF was calculated from the integrated intensities of (200), (211) and (311) austenite peaks and (002), (112) planes of ferrite. Then, the volume fraction of martensite ($V_M=1-V_\gamma-V_{BF}$, V_γ is volume fraction of austenite) and that of BF ($V_{BF}=1-V_\gamma-V_M$) were determined by point counting on SEM. Moreover, carbon content in retained austenite was calculated by using the relationship between lattice parameter and chemical composition shown in Ref. [11], and it should be noted that this relationship was selected because it is the most complete in terms of studying the influence of different elements on the austenite lattice parameter. Thus, it is possible to make out the carbon content in retained austenite and BF by using the austenite lattice parameter obtained by X-ray diffraction.

2 Results and Discussion

2.1 Morphology of NANOBAIN at different temperatures

It is well-known that mechanical properties of bainite depend on bainite plate size and retained austenite. The block retained austenite would have transformed into martensite under the influence of external stress or temperature before bainite reaction[1,12]. Fig. 1 shows the micrographs obtained under different isothermal transformation temperatures. Microstructure mainly consists of BF and retained austenite. Retained austenite exists in two types: film and block austenite. The latter is usually described as triangular shaped grains surrounded by crystallographic variants of bainite sheaves[13] while the former is much finer than the spatial resolution limit of SEM equipment. The majority observation is that the BF plate becomes more refined while lowering the temperature. Figs. 1(a)—1(c) show that both size and the amount of block austenite decreased with decreasing temperature except that obtained at 180 ℃ shown in Fig. 1(d). Retained austenite at 180 ℃ is several times more than that at other temperatures (210, 250, and 300 ℃) due to the fact that the time needed for the completion of bainite transformation at 180 ℃ should be long enough. In general, bainite transformation time at 210, 250, and 300 ℃ is 58.2, 16.0 and 7.5 h respectively[14] while the transformation time at 180 ℃ may exceed 8—10 days[1,15].

Block retained austenite consists of triangular and

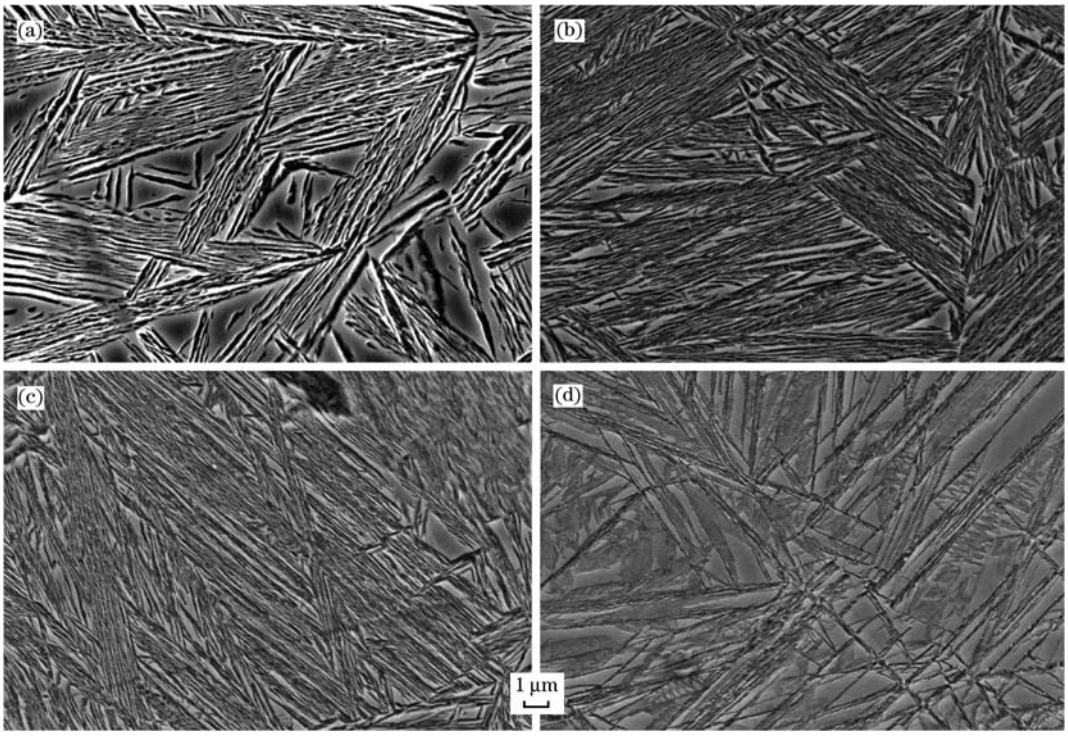

(a) 300 ℃ for 12 h; (b) 250 ℃ for 48 h; (c) 210 ℃ for 96 h; (d) 180 ℃ for 120 h.

Fig. 1 Scanning electron micrographs (SEM) of microstructure after transformation under different conditions

strip shaped grains. Though the size of triangular shaped grains at 180 ℃ are nearly the same as ones transformed at 300 ℃ (about 2.5 μm), the strip shaped grains transformed at 300 ℃ can also reach up to 10 μm like the ones transformed at 180 ℃. Moreover, it had been reported[16] that the ratio of film type retained austenite volume fraction V_γ(films) to that of blocky type austenite V_γ(block) can be calculated from the following expression, $V_\gamma(\text{films})/V_\gamma(\text{block})=(0.15V_{BF})/(V_\gamma-0.15V_{BF})$. In general, film austenite is much more stable than block austenite because of higher carbon content[17] and a large film/block austenite ratio, resulting in better toughness[18]. From Fig. 1, it can be concluded that transformation at extremely low temperature for enough time would generate higher volume fraction of BF and film retained austenite and lower amount of block retained austenite. The evolution of retained austenite fraction and carbon distribution as bainite transformation progresses at different isothermal temperatures will be discussed in the following content.

2.2 TEM examination

Typical microstructure of samples obtained at different temperatures for different time was examined by TEM. Fig. 2 shows TEM images of microstructure, in which the lighter microstructure is BF and the darker is film retained austenite. In addition, it should be noted that the existence of carbide has not been found because of the addition of silicon which suppresses the precipitation of carbide[10]. Lower bainite tends to form as aggregates (sheaves) of small platelets or plates (subunits) of ferrite[19]. Platelets within a sheaf consist of bainitic ferrite transformation units, namely, shear transformation units have regular parallelogram shape with average size of 84 nm×(40—160) nm seen in Fig. 2(a). Yu and Wang[20] observed two models of arrangement of shear transformation units in subunits: the transformation units of subunits are arranged in the same direction or are piled up symmetrically in two directions. The orientation of the former shows K-S relationship, and the basic shear transformation units are thought to be formed through invariant plane strain (IPS) with regular shape and definite habit plane. Hence, as for the process of BF growth, small ferrite subunits nucleated at the carbon depletion regions in the vicinity of austenite grain boundaries in the form of side-by-side fashion as seen in Fig. 2(d). Taylor et al.[21] reported that in Fe-Ni-C ageing martensite, there were carbon clusters with a modulated structure consisting of alternating carbon-poor and carbon-rich bands. And the carbon atom clustering process can be explained by a spinodal

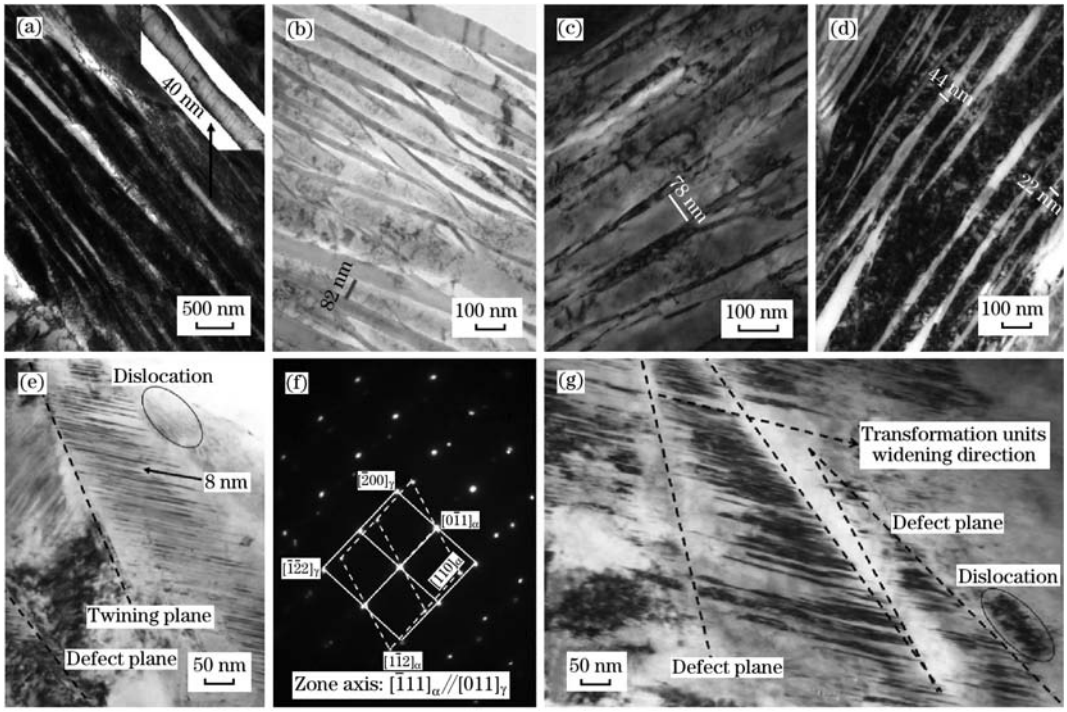

(a) 300 ℃ for 12 h; (b) 250 ℃ for 48 h; (c) 210 ℃ for 96 h; (d) 180 ℃ for 120 h; (e) Nano-scale twins in retained austenite of (c); (f) Corresponding diffraction pattern of (e); (g) Bainite/austenite interface and transformation units of (b).

Fig. 2 Transmission electron micrographs (TEM) of microstructure obtained under different conditions

decomposition mechanism. The inhomogeneity of BF morphology, i. e., the plate-like BF and granular BF mainly related to the different carbon contents of the adjacent retained austenite. The formation of carbon-enriched (overstabilized) and carbon-depleted (low-stability) retained austenite is associated well with the inhomogeneous bainite morphology[22]. The supersaturated carbon atoms ejected into the austenite build up at the interphase boundary and nucleated on the invariant shear planes in the form of interphase precipitation within BF shown in Fig. 2 (c). Fig. 2(b) indicates that BF subunits are most prominent near the edge or tip of another ferrite subunits where the impingement effect is minimal. The width of a subunit near the nucleation site is the same as that near the edge or tip of a sheaf, indicating that subunits grow to be a limited size[23]. Hence, in the process of BF transformation, small ferrite subunits mostly nucleated near the tips of subunits on just one side of each sheaf rather than on both sides as shown in Fig. 2(b). In addition, the thickening of sheaves formed from both sides of the habit plane[24]. Kang[25] also proposed that the lengthening of plate is in the course of the formation of new shear transformation units at both ends of bainite. A high stress-strain field in the parent phase around tips tends to generate sharp tips at both ends of the bainite plates, resulting in that the lengthening rate of bainite is much greater than that of thickening/widening. Hence, the three-dimensional morphology of bainite is a lengthened thin convex lens-like plate, as shown in Figs. 2(a) and 2(d).

It is well acknowledged that though the aspect ratio (thickness/length) and thickness of sheaves decrease with the decrease of transformation temperature and austenite grain size[14], it is not sensitive to the substitution alloy content[24]. Combining SEM and TEM micrographs, the effect of temperature on the microstructure especially the plate thickness in NANOBAIN steel is illustrated in Table 2 in detail. However, crystallographic theories of martensite show that the shape deformation is an invariant plane strain with a relatively large shear component[26]. The strain energy scales with the aspect ratio (thickness/length) upon the condition that the shape strains accommodate elastically, resulting in a thin plate to minimize the strain energy and volume of transformation per plate. In ideal circumstances, the driving force is the same as that of the strain energy, hence the decrease of transformation temperature can lead to the increase of thickness while the austenite stabilizing elements, such as carbon or man-

Table 2 Quantitative data on microstructure after isothermal transformation at room temperature

Temperature/℃	V_{BF}/%	V_γ(block)/%	V_γ(films)/%	V_M/%	BF plate thickness range/nm	Average plate thickness/nm
300	47±3	45±2	8±1	—	43—175	105±6
250	65±4	23±1	12±2	—	21—130	77±5
210	68±4	19±1	13±3	—	17—96	56±3
180	33±2	48±2	6±1	13±3	18—60	35±3

ganese decrease the width of plates[27]. BF subunits are connected platelets in parallel formations, indicating that the spacing between the platelets is to a large extent controlled by the carbon atoms diffusion field and the presence of adjacent palates; therefore, the extremely low temperature and high carbon content alloy can form the nanostructure BF plates, as seen in Fig. 2(e). Moreover, dislocation debris incited by the plastic deformation due to weakness of austenite at high temperature will eventually block the transformation interface, which lose the coherency. Hence, plates of bainite are easily arrested by dislocation (Fig. 2(e)) and austenite grain boundary even their size is much smaller than that of the austenite grain size[16,19].

The key feature of deformation in bainite is the accommodation twinning, which is different from these mechanical twinning found in martensite on account of the difference of austenite yield strength[27,28]. Accommodation twinning and its twinning plane is shown in the plates in Fig. 2(e), illustrating that the austenite exhibits extensive lenticular twinning with a thickness of about 2.5—12.0 nm. Fig. 2(f) demonstrats that the BF obeys the Nishiyama-Wasserman (N-W) orientation relationship with austenite and inherits twins from austenite as shown in the corresponding diffraction pattern. It was once pointed out that bainitic ferrite plates are close to the N-W orientation relationship with their parent austenite[5,29]. Sandvik[30] proposed that dislocation density in BF and twinning density in austenite increased with the decrease of transformed temperature. Deformation twin or twin zone often exists in high temperature austenite. Hence, BF directly inherits twinning from high-temperature austenite to generate sub-plate with Nishiyama-Wasserman (N-W) orientation relationship. The trace of nanoscale twinning verifies that the plastic deformation occurs in the surrounding austenite to accommodate the transformation strain as BF growth progresses[9]. The close relationship between BF and defects like twinning and dislocation can also be found in Fig. 2(g). It is concluded that the growth of transformation units is controlled by the defect plane surrounding with dislocation, which is consistent with the moving direction of BF/austenite interface parallel to the twinning plane. In summary, twinning in film austenite formed as a result of stress accommodation.

2.3 Mechanical properties

Fig. 3(a) shows the true strain-true stress curves at room temperature. The contribution of strength is mainly due to the very small thickness of BF plates and their high dislocation density may provide a maximum stress of 500 MPa[31]. The contribution of yield strength caused by BF plates is given by $\Delta\sigma =$

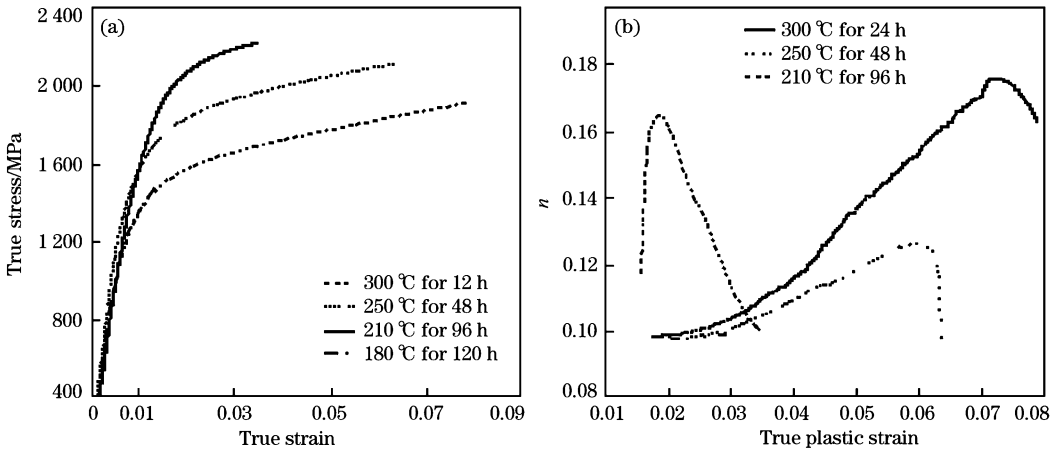

Fig. 3 True strain-true stress curves at different temperatures (a) and corresponding work hardening exponent as a function of true plastic strain (b)

$57.5(\overline{L})^{-1}$, where $\overline{L}$ is the average plate thickness[14] in micrometers. It is obviously understood that the main contribution yield strengths of BF plates are 564 MPa, 747 MPa, and 1026 MPa respectively with the decrease of transformation temperature. The mechanical properties obtained at different temperatures are shown in Table 3. The strength increases with the decrease of temperature while the total elongation is quite opposite to the strength trend except that at 180 ℃.

This behavior is related to microstructural features at different transformation temperatures. Microstructure transformed at 180 ℃ for 120 h consists of little BF, massive retained austenite and martensite, as shown in Table 2. More austenite could enhance ductility while martensite would severely decrease it[24,25]. On the other hand, the soft phase retained austenite seems to have a close relationship with the ductility, and the stability of retained austenite against straining also affects the uniform elongation[32].

Table 3 Summary of experimental data from tensile tests at room temperature

T/℃	t/h	YS/MPa	UTS/MPa	ε_T/%
300	12	1190	1620	12
250	48	1270	1860	8
210	96	1600	2070	6
180	120	—	1460	4

Note: T, t and ε_T stand for the isothermal transformation temperature, heat treatment time, and the total elongation, respectively.

Work hardening behavior as a function of true plastic strain versus incremental work hardening exponent is shown in Fig. 3(b). The result reveals a similar behavior such as a slow increase of n during the first deformation stage followed by a dramatic drop that ends compared with both steels obtained at 300 and 250 ℃. Steel transformed at 300 ℃ shows better work hardening behavior due to the existence of more block retained austenite which has the tendency of transforming into martensite during the deformation. However, the curve of the sample transformed at 210 ℃ rapidly increases at a very small strain, demonstrating that the microstructure with little block and much thin film retained austenite show little benefit to strain transformation. It also confirms that the mechanical stability of microstructure obtained at 250 ℃ and 300 ℃ is much more stable than that at 210 ℃, which is determined by the block morphology of retained austenite and chemical composition like carbon content[33].

2.4 Retained austenite and carbon distribution analyzed by XRD

It is widely acknowledged that BF transformation rate is low when the transformation temperature is reduced below 200 ℃. Hence, the time of isothermal treatment at low temperature seems to be more critical for the combination of high strength and good ductility. The amount of retained austenite measured by quantitative X-ray analysis versus elongation is shown in Fig. 4. It is obvious that the total elongation is determined by the fraction of retained austenite especially the amount of block retained austenite, in the condition that the transformation of BF is nearly completed. Otherwise, the transformation fraction of BF is so little at extremely low temperature such as 180 ℃, while detrimental martensite is easily to form, which results in a low elongation. A longer heat-treatment period is beneficial to generate much more BF, but not to the improvement of total elongations, and a lower temperature is helpful to reach the maximum extent of BF transformation if the time is not limited.

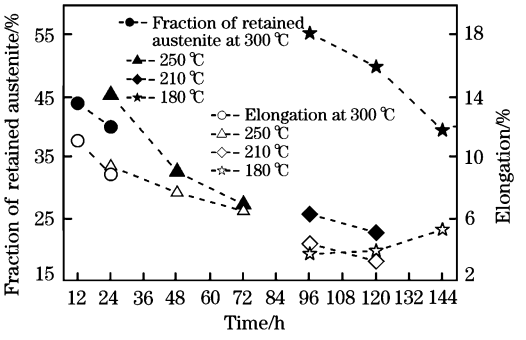

Fig. 4 Evolution of fraction of retained austenite and elongation as bainite transformation progresses at different temperatures

The carbon content in retained austenite was estimated by the well-known Dyson and Holmes' equation, which shows the relationship between the austenite lattice parameter and its composition[11]. The carbon content in BF was calculated by the carbon content in retained austenite according to mass conservation in principle[1]. It should be noted that difference of carbon content between block and thin film retained austenite could not be distinguished by the analysis of XRD. And generally the austenite films entrapped between neighboring sub-units of BF have a higher carbon content than the block residual austenite located between the sheaves of BF[34].

Such thin film austenite can continue to accumulate carbon from the isolated new supersaturated BF within the range between the T'_0 (carbon equilibrium concentration between austenite and retained austenite when bainite stored energy is 400 J·mol^{-1}) value (7.50 at. %) and A'_{e3} (phase equilibrium temperature between austenite and BF) value (21.00 at. %)[35].

The evolution of carbon partitioning in retained austenite and BF with bainite transformation at 250 ℃ is shown in Fig. 5. Retained austenite is gradually enriched in carbon (increased from 6.20 at. % to 7.30 at. %) at the initial stage, likely caused by the formation of BF which makes the excess carbon atom diffuse into austenite[36]. Subsequently, after the formation of BF, austenite is not greatly enriched in carbon and carbon content shows a little decrease instead (decreased from 7.28 at. % to 6.10 at. % at 250 ℃, and from 5.80 at. % to 5.50 at. % at 300 ℃), which may be caused by the BF interface which trapped a significant amount of carbon. The bainite reaction is expected to cease if the carbon content in austenite reaches the value at which transformation becomes thermodynamically impossible[1]. However, the carbon content of retained austenite at 210 and 180 ℃ was lower than that at 250 and 300 ℃, and retained austenite is gradually enriched in carbon with holding time. The carbon content in retained austenite at 210 ℃ is consistent with Refs. [10,36]. As for the evolution of carbon content in retained austenite transformed at 210 and 180 ℃, it may be due to the fact that some BF plates formed early in the transformation process and there was more time (>144 h) for carbon diffusion back into the austenite.

The carbon content in BF (varied from 0.40 at. % to 2.90 at. %) is much higher than the para-equilibrium

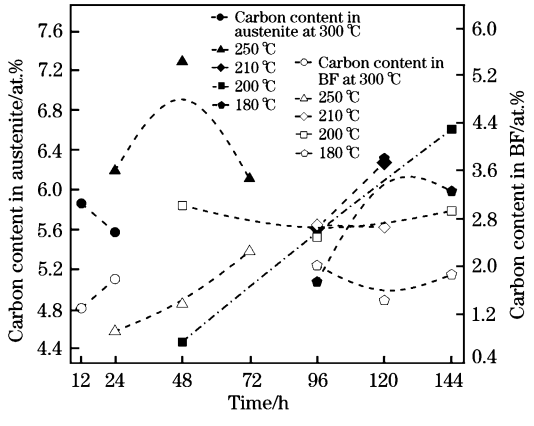

Fig. 5 Evolution of the carbon partitioning in retained austenite and BF during bainite transformation

value (0.12 at. %) during bainite transformation at lower temperature. The carbon in BF transformed at 300 and 250 ℃ seems to accumulate more, which may be due to the fact that the relatively high density dislocation is an advantageous region for the carbon to be trapped and austenite/bainite interface is carbon-enriched region. The average carbon level of the Cottrell atmosphere dislocation debris caused by the plastic deformation was estimated to be (13.40±0.80) at. %, which is higher than previous experimental content of carbon trapped at dislocations in the vicinity of ferrite/austenite interface which was estimated to be (7.40±0.10) at. %[37]. Carbon is easily to be trapped at crystal defects to prevent the decarburization of supersaturated BF and therefore alters the carbide precipitation sequence during low-temperature bainite transformation[37]. Moreover, a phenomenon of little decarburization of supersaturated BF has been found as the bainite transformation progresses but the carbon precipitation does not occur at the extremely low temperature (210 ℃ and 180 ℃) and long heat treating time (>96 h). This is more likely as it is such an uniform zone (carbon content in BF varied from 1.40 at. % to 2.00 at. %), which is consistent with Refs. [10,36]. There is no carbon content variation between such BF plates due to the fact that some plates formed early in the transformation process and there was enough time for carbon diffusion back into the austenite.

3 Conclusions

(1) The formation process of BF was complicated and diverse, and the BF made of basic shear transformation units is arranged in the same direction of subunits at 300 ℃. TEM images indicated that the lengthening of BF plates are caused by the formation of new shear transformation units at both ends of the BF.

(2) The existence of defect like nanoscale twinning and dislocation shows that the growth of transformation units is controlled by the surrounding defect plane with dislocation, which is consistent with the moving direction of BF/austenite interface parallel to the twinning plane.

(3) The behavior of work hardening proves that mechanical stability of microstructure obtained at 250 ℃ and 300 ℃ is much more stable than that at 210 ℃, which is eventually determined by the block morphology of retained austenite and its carbon content.

(4) The evolution of the carbon partitioning in

retained austenite and BF with the bainite transformation can be concluded that austenite is gradually enriched in carbon at the initial stage; after the formation of BF, austenite is not greatly enriched in carbon, and the carbon content shows a little decrease instead; subsequently, a phenomenon of little decarburization of supersaturated BF has also been found; however, the carbon precipitation does not occur during the transformation progress.

References:

[1] Y. Huang, A. Zhao, J. He, X. Wang, Z. Wang, L. Qi, Int. J. Min. Met. Mater. 20 (2013) 1155-1163.

[2] Y. Huang, Z. Zhao, A. Zhao, W. Sun, K. Bao, J. Univ. Sci. Technol. B. 7 (2013) 882-889.

[3] X. Wang, A. Zhao, Z. Zhao, Y. Huang, L. Li, Q. He, Int. J. Min. Met. Mater. 21 (2014) 266-272.

[4] C. Garc I. A. Mateo, F. Garc, I. A. Caballero, H. Bhadeshia, ISIJ Int. 8 (2003) 1238-1243.

[5] H. Beladi, Y. Adachi, I. Timokhina, P. D. Hodgson, Scripta Mater. 60 (2009) 455-458.

[6] H. Bhadeshia, Mater. Sci. Eng. A. 378 (2004) 34-39.

[7] J. Seol, D. Raabe, P. Choi, Y. Im, C. Park, Acta Mater. 60 (2012) 6183-6199.

[8] Y. Huang, A. Zhao, Z. Mi, H. Jing, W. Li, Y. Hui, J. Iron Steel Res. Int. 20 (2013) No. 11, 111-117.

[9] F. G. Caballero, H. Yen, M. K. Miller, J. Yang, J. Cornide, C. Garcia-Mateo, Acta Mater. 59 (2011) 6117-6123.

[10] F. G. Caballero, M. K. Miller, A. J. Clarke, C. Garcia-Mateo, Scripta Mater. 63 (2010) 442-445.

[11] D. J. Dyson, B. Holmes, J. Iron Steel Int. 208 (1970) 469-474.

[12] K. Hase, C. Garcia-Mateo, H. K. D. H. Bhadeshia, Mater. Sci. Eng. A. 438 (2006) 145-148.

[13] C. Garcia-Mateo, F. G. Caballero, J. Chao, C. Capdevila, C. G. de Andres, J. Mater. Sci. 44 (2009) 4617-4624.

[14] C. Garc I. A. Mateo, F. Garc, I. A. Caballero, H. Bhadeshia, ISIJ Int. 11 (2003) 1821-1825.

[15] M. N. Yoozbashi, S. Yazdania, Solid State Phenomena. 172 (2011) 214-220.

[16] H. Bhadeshia, D. V. Edmonds, Met. Sci. 17 (1983) 411-419.

[17] C. Garcia-Mateo, F. G. Caballero, C. Capdevila, C. Andres, Scripta Mater. 61 (2009) 855-858.

[18] H. Bhadeshia, D. V. Edmonds, Met. Sci. 17 (1983) 420-425.

[19] H. Bhadeshia, J. W. Christian. Metall. Mater. Trans. A 21 (1990) 767-797.

[20] D. G. Yu, S. D. Wang, Therory of the Bainite Transformation, Shanghai Jiaotong University Press, Shanghai, 1998.

[21] K. A. Taylor, G. B. Olson, M. Cohen, J. B. V. Sande, Metall. Mater. Trans. A 20 (1989) 2749-2765.

[22] I. B. Timokhina, H. Beladi, X. Y. Xiong, Y. Adachi, P. D. Hodgson, Acta Mater. 59 (2011) 5511-5522.

[23] H. K. D. H. Bhadeshia, D. V. Edmonds, Metall. Mater. Trans. A 10 (1979) 895-907.

[24] G. R. Speich, W. C. Leslie, Metall. Mater. Trans. A 3 (1972) 1043-1054.

[25] M. Kang, M. Zhang, M. Zhu, Acta Mater. 54 (2006) 2121-2129.

[26] J. W. Christian, Acta Mater. 6 (1958) 377-379.

[27] L. C. Chang, H. Bhadeshia, Mater. Sci. Technol. Lond. 11 (1995) 105-108.

[28] L. Duprez, B. C. D. Cooman, N. Akdut, Metall. Mater. Trans. A 7 (2002)1931-1938.

[29] M. X. Zhang, P. M. Kelly, Mater. Sci. Eng. A 438 (2006) 272-275.

[30] B. P. J. Sandvik, Metall. Mater. Trans. A 13 (1982) 777-787.

[31] H. Bhadeshia, R. Honeycombe, Steels: Microstructure and Properties: Microstructure and Properties, 2nd ed., Butterworth-Heinemann, New York, 1995.

[32] K. Sugimoto, N. Usui, M. Kobayashi, S. Hashimoto, ISIJ Int. 32 (1992) 1311-1318.

[33] C. Garcia-Mateo, F. G. Caballero, Mater. Trans. 8 (2005) 1839-1846.

[34] F. G. Caballero, C. Garcia-Mateo, M. J. Santofimia, M. K. Miller, C. García De Andrés, Acta Mater. 57 (2009) 8-17.

[35] C. Garcia-Mateo, F. G. Caballero, M. K. Miller, J. A. Jimenez, J. Mater. Sci. 47 (2012) 1004-1010.

[36] F. G. Caballero, M. K. Miller, C. Garcia-Mateo, Acta Mater. 58 (2010) 2338-2343.

[37] F. G. Caballero, M. K. Miller, S. S. Babu, C. Garcia-Mateo, Acta Mater. 55 (2007) 381-390.